




Article

# Well Defined Poly(Methyl Methacrylate)- Fe<sub>3</sub>O<sub>4</sub>/Poly(Vinyl Pivalate) Core–Shell Superparamagnetic Nanoparticles: Design and Evaluation of In Vitro Cytotoxicity Activity against Cancer Cells

Graciane Resende <sup>1</sup>, Gabriel V. S. Dutra <sup>1</sup>, Maria S. B. Neta <sup>2</sup>, Olacir A. Araújo <sup>3</sup> ,  
Sacha B. Chaves <sup>2</sup>  and Fabricio Machado <sup>1,\*</sup> 

<sup>1</sup> Laboratório de Desenvolvimento de Processos Químicos, Instituto de Química, Universidade de Brasília, Campus Universitário Darcy Ribeiro, CEP 70910-900 Brasília, DF, Brazil; graciane.resende@aluno.unb.br (G.R.); gabriel.victor@aluno.unb.br (G.V.S.D.)

<sup>2</sup> Departamento de Genética e Morfologia, Instituto de Biologia, Universidade de Brasília, Campus Universitário Darcy Ribeiro, CEP 70910-900 Brasília, DF, Brazil; sousa.brito@aluno.unb.br (M.S.B.N.); sachabraun@unb.br (S.B.C.)

<sup>3</sup> Universidade Estadual de Goiás, Campus Central—Ciências Exatas e Tecnológicas, CP 459, CEP 75132-903 Anápolis, GO, Brazil; olacir.araujo@ueg.br

\* Correspondence: fmachado@unb.br or fabricio.machado@nottingham.ac.uk; Tel.: +55-61-3107-3868

† Current address: School of Chemistry, University of Nottingham, University Park, Nottingham NG7 2RD, UK.

Received: 24 October 2020; Accepted: 23 November 2020; Published: 30 November 2020



**Abstract:** The objective of this work is to develop and characterize polymeric nanoparticles with core–shell morphology through miniemulsion polymerization combined with seeded emulsion polymerization, aiming at the application in the treatment of vascular tumors via intravascular embolization. The synthesis of the core–shell nanocomposites was divided into two main steps: (i) Formation of the core structure, consisting of poly(methyl methacrylate)/magnetic oxide coated with oleic acid (OM-OA) via miniemulsion and (ii) shell structure produced through seeded emulsion polymerization of vinyl pivalate. Nanocomposites containing about 8 wt.% of OM-OA showed high colloidal stability, mean diameter of 216.8 nm, spherical morphology, saturation magnetization ( $M_s$ ) of  $4.65 \text{ emu}\cdot\text{g}^{-1}$  ( $57.41 \text{ emu}\cdot\text{g}^{-1}$  of  $\text{Fe}_3\text{O}_4$ ), preserved superparamagnetic behavior and glass transition temperature ( $T_g$ ) of  $111.8 \text{ }^\circ\text{C}$ . TEM micrographs confirmed the obtaining of uniformly dispersed magnetic nanoparticles in the PMMA and that the core–shell structure was obtained by seeded emulsion with  $M_s$  of  $1.35 \text{ emu}\cdot\text{g}^{-1}$  ( $56.25 \text{ emu}\cdot\text{g}^{-1}$  of  $\text{Fe}_3\text{O}_4$ ) and  $T_g$  of  $114.7 \text{ }^\circ\text{C}$ . In vitro cytotoxicity assays against murine tumor of melanoma (B16F10) and human Keratinocytes (HaCaT) cell lines were carried out showing that the core–shell magnetic polymeric materials (a core, consisting of poly(methyl methacrylate)/ $\text{Fe}_3\text{O}_4$  and, a shell, formed by poly(vinyl pivalate)) presented high cell viabilities for both murine melanoma tumor cell lines, B16F10, and human keratinocyte cells, HaCaT.

**Keywords:** methyl methacrylate; vinyl pivalate; magnetic nanoparticles; embolization; miniemulsion; seeded emulsion; core–shell polymer particles

## 1. Introduction

The development of polymeric materials is undoubtedly attractive in the manufacture of many biomedical devices, given their structural versatility, ease of manufacture, biocompatibility,

low cytotoxicity, flexibility, biodegradability, porosity, and controlled morphology, among others [1,2]. In this field, highlight the nanocomposites that combine the thermoplastic properties of polymers and the superparamagnetic behavior of nanoparticles, presenting great potential in the treatment of vascular tumors [3,4].

Iron oxide nanoparticles possessing various characteristics such as biocompatibility, superparamagnetic properties, and recyclability [5] have been widely used in controlled drug delivery systems, facilitating drug channeling to specific target cells by externally controlling their path using a field [6], and as a contrast agent for magnetic resonance, hyperthermia treatment of tumors and detoxification of biological fluids [7–9], etc.

In biomedical applications, the encapsulation of nanoparticles with polymeric matrices ensures their stability in biological media, provides functionality, protects and prevents agglomeration [10] and results in increased local drug concentrations, enabling their use for targeted delivery of therapeutic agents, reducing toxic effects in cells or tissues healthy [11,12]. The polymeric matrices can be prepared from synthetic or natural polymers, obtaining colloidal particles by several synthetic routes, including emulsion [13–15], suspension [16–18], and miniemulsion polymerization [19–21].

Embolization therapy involves deliberate blocking of blood vessels due to the introduction of embolic agents, with the aim of decreasing or preventing blood transport through the blood vessels towards the injured area [22]. The choice of the adequate embolizing agent is important for the safety and effectiveness of the treatment [23]. Embolic agents can be classified into two main categories: Temporary and permanent. Although temporary agents block blood flow, they will be dissolved or eliminated by the immune system within a prescribed period of time. For the temporary embolic materials, the most used materials are autologous agents and resorbable gelatin sponge. Permanent agents are designed to provide irreversible blood flow obstruction to target lesions or final organs. In particular for the permanent embolic agent, the most used materials are coils, plugs, detachable balloons (solid agents), polyvinyl alcohol, compressible microspheres, thrombin, dehydrated alcohol, sodium tetradecyl sulfate, glues, and onyx (liquid agents) [23,24].

The miniemulsion polymerization process has excelled in recent years due to the intrinsic characteristics of the materials obtained, such as narrow particle size distributions, high colloidal stability, high molar mass, obtaining a wide range of polymers and mainly, the ability to encapsulate materials inorganics in a single reaction step with fast polymerization rates [25–28]. A versatile class of nanocomposites can be developed by combining the peculiarities of the miniemulsion with other polymerization techniques, obtaining polymeric nanoparticles of the core–shell type, the core being produced from the polymer initially polymerized, and the polymers formed later are incorporated into the layer external [29]. These materials have final properties dependent not only on the composition of each polymeric phase, but also on the morphology of these particles [30].

Core–shell polymer nanoparticles have attracted great interest due to their unique structure in which two different components are combined into a single material [31]. In biological applications, core–shell nanoparticles have great advantages over conventional nanoparticles, thus improving performance, such as low cytotoxicity, good dispersibility, high biocompatibility and cell compatibility, better connection with other biologically active molecules, as well as improved thermal and chemical stability [6,32,33].

With this perspective, Rahman et al. [34] developed a thermo-responsive magnetic polymer, synthesizing the magnetic seeds of cross-linked polystyrene by emulsion polymerization. The thermosensitive poly(*N*-isopropylacrylamide) shell (PNIPAM) was obtained via precipitation polymerization and then the polymer was functionalized with aminoethylmethacrylate hydrochloride (AEMH). The TEM micrographs confirmed the core–shell morphology of the particles. Chen et al. [35] synthesized hybrid epoxy–acrylic latex with core–shell morphology, using an epoxy dispersion as seed and, subsequently, carried out the seeded emulsion polymerization in acrylic monomer. Recently, Li et al. [36] synthesized cross-linked polystyrene nanospheres via dispersion polymerization and, subsequently, these seeds were swollen in *tert*-butyl acrylate and styrene monomers and

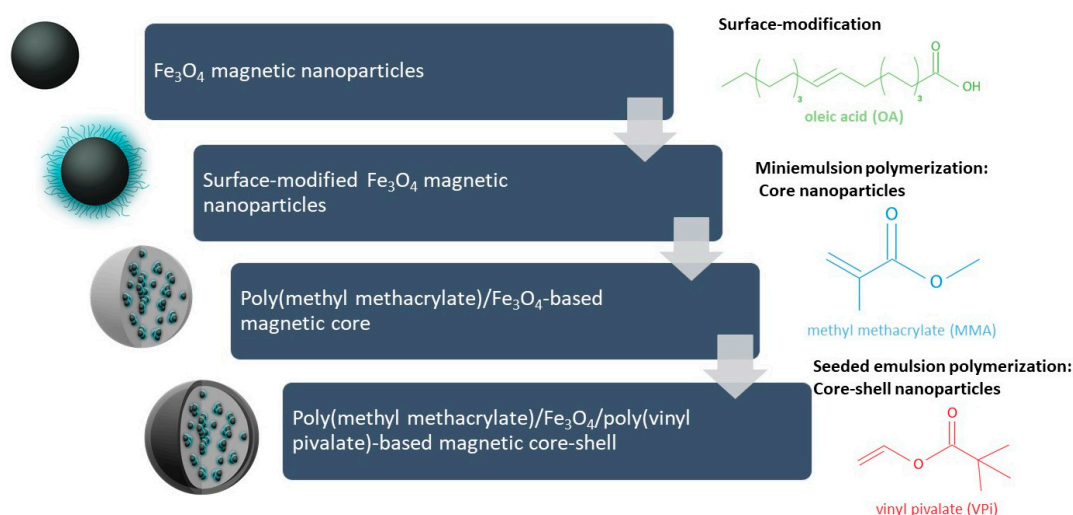
polymerized by seeded emulsion. The authors investigated the effect of methanol concentration, used in the synthesis of seeds, and the degree of crosslinking on the morphology of the nanoparticles.

For the synthesis of core–shell nanoparticles to be successful, the polymerization technique and the operating conditions used are highly fundamental [37]. In the current work, the technique used for the formation of the shell is the seeded emulsion, which consists of the formation of a new polymer layer grafted on the seed surface (N.B. herein, the core nanoparticles consisting of poly(methyl methacrylate)/Fe<sub>3</sub>O<sub>4</sub> is synthesized through miniemulsion polymerization process), through addition of fresh monomer feed following a semibatch mode operation, leading to the formation of a uniform shell and promoting easy control of final core–shell morphology [38,39].

The focus of this work is to obtain core–shell particles through combination of a batch mode (used to form the core structure via miniemulsion polymerization) and a semicontinuous mode operation (to form the particle shell structure through seeded emulsion polymerization), in which the feed composition is adequately controlled, allowing for the formation of a new polymer phase on the previously formed polymer particle. These particular core–shell polymer particles, intended for to be used as an embolic agent, consist basically of (i) a core, consisting of oleic acid functionalized magnetic nanoparticles (OM-OA), properly dispersed into spherical poly(methyl methacrylate) nanoparticles (PMMA), and (ii) a shell, consisting of poly(vinyl pivalate) (PVPi). By the combination of vinyl pivalate and methyl methacrylate, this new magnetic embolic agent based on PVPi/PMMA exhibits low susceptibility to undesirable hydrolysis reactions, which is strongly responsible for the recanalization of blood vessels, since they are minimized by the steric effect caused by the insertion of PVPi into the particles due to the tert-butyl group present in its chemical structure [17,40]. In addition, these nanocomposites have good chemical and mechanical resistance and high thermal stability, conferred to the methyl methacrylate based core [41]. As an additional study, the cytotoxicity of PVPi/PMMA core–shell particles was evaluated in vitro for tumoral cell lines B16F10 (murine melanoma) and HaCat (human keratinocyte). In vitro studies are of fundamental importance to give insight into the cytotoxicity ability of the magnetic nanocomposites on tumoral and non-tumoral cell lines. In the current work, B16F10 and HaCat were selected because murine B16F10 melanoma model is widely used as metastatic melanoma model for preclinical studies, as well as, human keratinocyte HaCaT cell line model is extensively used in epidermal homeostasis and pathophysiology studies.

## 2. Materials and Methods

All reagents were analytical grade (PA) and used without prior purification. Methyl methacrylate (MMA) 99%, vinyl pivalate (VPi) 99%, hexadecane 99%, benzoyl peroxide 75% and ethylene glycol dimethylacrylate (EGDMA) 98% were purchased from Sigma-Aldrich Brasil Ltda. (Rio de Janeiro, Brazil). Hydrochloric acid (HCl) 36.5–38% and oleic acid 99% were purchased from Synth (São Paulo, Brazil). Ferric chloride hexahydrate (FeCl<sub>3</sub>·6H<sub>2</sub>O) 97%, ferrous sulfate heptahydrate (FeSO<sub>4</sub>·7H<sub>2</sub>O) 99%, sodium hydroxide (NaOH) 99% and potassium persulfate (KPS) 99% were purchased from Vetec Química Fina Ltda. (Rio de Janeiro, Brazil) and 90% pure sodium dodecyl sulfate (SDS) was supplied by Reagen Produtos para Laboratórios Ltda. (Parana, Brazil). Nitrogen gas was supplied by White Martins Gases Industriais Ltda. (Rio de Janeiro, Brazil) with 99.5% purity. Scheme 1 illustrates the experimental protocol for the synthesis of poly(methyl methacrylate)/Fe<sub>3</sub>O<sub>4</sub>/poly(vinyl pivalate) magnetic core–shell nanoparticles.



**Scheme 1.** Flowchart summarizing the experimental protocol for formation of poly(methyl methacrylate)/Fe<sub>3</sub>O<sub>4</sub>/poly(vinyl pivalate) magnetic core-shell nanoparticles.

### 2.1. Synthesis of Magnetic Nanoparticles (OM)

Magnetic nanoparticles (OM) were obtained by the alkaline hydrolysis coprecipitation method of Fe<sup>2+</sup> and Fe<sup>3+</sup> ions in watery environment, as described by Neto et al. [42] in 500 mL of distilled water were added 2 mL of a 10% HCl solution and 0.03 mol of Fe<sup>2+</sup> and Fe<sup>3+</sup> metal ions in a stoichiometric molar ratio of 1:2 with 0.01 mol of FeSO<sub>4</sub>·7H<sub>2</sub>O and 0.02 mol of FeCl<sub>3</sub>·6H<sub>2</sub>O. The mixture was heated to 70 °C under constant stirring at 500 rpm and under nitrogen atmosphere for 30 min. Then the precipitating agent, NaOH, with a concentration of 5 mol L<sup>-1</sup> was added until the solution reached a pH of approximately 12. After precipitation, the suspension remained under stirring at 70 °C and bubbling nitrogen for 30 min. The precipitate was washed with distilled water and decanted with the aid of a magnet until it reached neutral pH.

### 2.2. Coating of Magnetic Nanoparticles with Oleic Acid (OM-OA)

The magnetic nanoparticles were suspended in 170 mL of distilled water and then subjected to mechanical stirring under nitrogen bubbling and 85 °C heating. Then the coating material, 2.5 mL oleic acid, was added dropwise at a maximum rate of 0.5 mL min<sup>-1</sup>. After 30 min of the addition of oleic acid, the nanoparticles were washed with distilled water to neutral pH and treated with acetone to remove free coating material [16,42].

### 2.3. Synthesis of PMMA/OM-OA Magnetic Nanocomposite

For the production of nanocomposites, different parameters such as temperature, reaction time, amount of initiator and OM-OA content were studied. The concentration of surfactant, SDS, used in the synthesis was below the critical micellar concentration (CMC) at a temperature of 85 °C, which corresponds to 4.35 g L<sup>-1</sup> [43] and 3.68 g L<sup>-1</sup> at 70 °C (N.B. different from emulsion polymerization process, the amount of surfactant is kept below CMC in order to avoid the formation of micelles in the continuous aqueous phase, which guarantees that the polymerization reactions take place preferably inside the monomer nanodroplets).

The nanocomposite was synthesized by miniemulsion polymerization as follows: In one case the aqueous phase was homogenized with 153 g of distilled water and 0.6 g of SDS under constant stirring at 300 rpm for 10 min. Separately, the organic phase consisting of 27 g MMA, 0.81 g hexadecane, 0.72 g BPO and 4.05 g OM-OA was prepared in a beaker and homogenized using an ultrasonic disperser (Cole-Parmer® 750 W, Vernon Hills, IL, USA) for 5 min at 40% amplitude in an ice bath. Subsequently, the organic phase was mixed into the aqueous phase and kept under constant stirring at 2700 rpm

for 20 min in a mechanical disperser (IKA T25 digital ULTRA TURRAX<sup>®</sup>, Wilmington, NC, USA). Then the mixture was homogenized again through the ultrasonic disperser for 4 min at 70% amplitude in an ice bath. Finally, the mixture was added to a jacketed reactor at 85 °C and maintained by constant stirring at 400 rpm for 2 h.

#### 2.4. Production of Poly(Vinyl Pivalate) Shell via Seeded Emulsion Polymerization

Core-shell morphology nanoparticles (PMMA/OM-OA/PVPi) were obtained using the seeded emulsion method [44], where PMMA/OM-OA nanocomposite seeds were fed with vinyl pivalate (VPi), initiator (KPS), and cross-linking agent (EGDMA) for shell formation. In a 500 mL tritubulated flask was added 200 g of PMMA/OM-OA colloidal dispersion (N.B. mass fraction of PMMA/OM-OA nanoparticles equal to 13.6%). The main components of the seeded emulsion polymerization step were initially separated into two phases, added separately into the PMMA/OM-OA colloidal dispersion: (i) The organic phase consisting of approximately 5.155 g VPi and 0.103 g EGDMA and (ii) the aqueous phase 20.5 g distilled water, 0.12 g SDS and 0.103 g KPS. The PMMA/OM-OA colloidal dispersion was kept under constant agitation at 500 rpm at 70 °C. Organic phase feeding was performed using a Solenoid Metering pump (ProMinent<sup>®</sup>, Gala series gamma/L 1000, São Paulo, Brazil) with a rate of 2.56 g h<sup>-1</sup>. After 1h of feeding the organic phase, the aqueous phase was slowly added for about 1 h. Then the remainder of the organic phase was added at the same rate. Subsequently, the polymerization was maintained for a further 2 h at 70 °C in inert nitrogen atmosphere.

#### 2.5. Sample Characterization

X-ray diffraction measurements were used to identify the crystallographic phases present in the dimensions and the average size of the crystals. The diffractograms were acquired using a Rigaku-D/MAX X-Ray diffractometer (Austin, TX, USA), with CuK $\alpha$  ( $\lambda = 1.542510 \text{ \AA}$ ) as a radiation source and a Ni-filtrate with CBO monochromator operating at 35 kV and 15 mA. The measurements performed in the variation range of  $25^\circ \leq 2\theta \leq 80^\circ$  with an increment of  $0.05^\circ$  and angular velocity of  $1.0^\circ \text{ min}^{-1}$ .

The magnetization measurements were obtained using a vibrating sample magnetometer (VSM, MicroSense, Lowell, MA, USA), ADE Magnetics model EV-9, with a magnetic field from -18 to +18 (kOe), at room temperature.

Energy dispersive X-ray spectroscopy (EDX) analyses measurements were carried out on an EDX-720 fluorescence spectrometer (Shimadzu Europa GmbH, Duisburg, Germany). EDX spectra were acquired under vacuum with a 10 mm collimator at accelerating voltage of 50 keV with steps of 0.02 and a live time of 100 s, using the Ti-U channel.

Fourier transform infrared spectra (FTIR) were displayed by dispersing bottles in KBr and presented as pellets. The spectra were acquired on a Varian Model 640 spectrometer (Varian Instruments, Santa Clara, CA, USA) with a resolution of  $4 \text{ cm}^{-1}$ , updating 16 scans per sample.

The average diameter of monomer droplets ( $D_g$ ) and polymeric particles ( $D_p$ ) were determined using the dynamic light scattering technique (DLS) using a Malvern model Zetasizer Nano ZS (Malvern Instruments Ltd, Malvern, UK). For the analyzes, the samples were diluted with distilled water.

Transmission electron micrographs (TEM) were obtained using a JEOL JEM-2100 (Jeol Ltd., Tokyo, Japan) microscope operated at 200 kV. The samples were dispersed in water and sonicated for 5 min, where a drop of the suspension was applied on a copper screen containing a 200 mesh supported carbon film and dried at room temperature. The differential scanning calorimetry (DSC) curves were obtained using a Shimadzu equipment (model DSC-60, Shimadzu Scientific Instruments, Columbia, MD, USA). The initial masses used were approximately 5.0 mg and aluminum crucibles were used. For analysis, two heating ramps were performed, using a temperature range of -30 to 180 °C, with a temperature ramp of  $10 \text{ }^\circ\text{C}\cdot\text{min}^{-1}$ , He flow of  $30 \text{ mL}\cdot\text{min}^{-1}$  and cooling was performed using liquid N<sub>2</sub>. The second heating ramp was used to determine the glass transition temperature ( $T_g$ ) of the nanocomposites.

The conversions were determined by gravimetry, and the latexes were added in previously weighed aluminum foil capsules, treated with  $2 \text{ g}\cdot\text{L}^{-1}$  hydroquinone solution and dried in an oven at  $60 \text{ }^\circ\text{C}$  for approximately 48 h. The conversion was obtained by the ratio of the dry polymer mass to the monomer mass used.

### 2.6. In Vitro Cytotoxicity Assays

The polymer materials were evaluated through in vitro cytotoxicity tests with murine melanoma (B16F10) and human keratinocyte (HaCat) tumor lines provided by Cell Bank of Rio de Janeiro, Brazil and maintained in culture at Nanobiotechnology Laboratory of the University of Brasília, UnB. All cell lines were cultured in DMEM (Dulbecco's Modified Eagle Medium, provided by Sigma-Aldrich Brasil, São Paulo, Brazil) medium buffered with sodium bicarbonate and supplemented with 1% antibiotic ( $100 \text{ IU}\cdot\text{mL}^{-1}$  penicillin and  $100 \text{ }\mu\text{g}\cdot\text{mL}^{-1}$  streptomycin) and 10% fetal bovine serum (FBS) at pH 7.2. Cells were maintained in cell culture flasks into an incubator at  $37 \text{ }^\circ\text{C}$ , under 95% humidified air and 5%  $\text{CO}_2$  atmosphere, and the assays were performed in the logarithmic growth phase of the cells. Viable cells were quantified by using  $40 \text{ }\mu\text{L}$  of solution of Trypan Blue dye added in 10 microliters of cell suspension. The samples were evaluated for 24 h, with concentrations equal to  $0.01 \text{ mg}\cdot\text{mL}^{-1}$ ,  $0.05 \text{ mg}\cdot\text{mL}^{-1}$ ,  $0.1 \text{ mg}\cdot\text{mL}^{-1}$ ,  $0.25 \text{ mg}\cdot\text{mL}^{-1}$ , and  $0.5 \text{ mg}\cdot\text{mL}^{-1}$ . The tumor cell lines (B16F10 and HaCat) were seeded in 96-well plates at a concentration of  $2\cdot 10^3$  and  $5\cdot 10^3$  cells per well with DMEM medium. Cell viability was determined by using the 3-(4,5-dimethylthiazol-2-yl)-2,5-diphenyl tetrazolium bromide-reducing colorimetric method (MTT) through spectrophotometry measurements using a 595 nm wavelength, whose results correspond to an average of three independent experiments in triplicates.

## 3. Results and Discussion

Figure 1 shows the powder X-ray diffractograms and their diffraction patterns of OM and OM-OA samples. All peaks were analyzed and compared using data from the Joint Committee on Powder Diffraction Standards (JCPDS). The characteristic peaks of magnetic particles were observed at  $2\theta = 30.2^\circ$ ,  $35.6^\circ$ ,  $43.3^\circ$ ,  $53.6^\circ$ ,  $57.3^\circ$ ,  $62.8^\circ$ , and  $74.5^\circ$ , respectively, corresponding to the reflections of the crystalline planes (220), (311), (400), (422), (511), (440), and (533) of typical magnetite and/or maghemite spinel type cubic crystal structure. The diffraction patterns of the samples were similar, showing that the presence of oleic acid did not influence the structural and crystalline properties of nanoparticles [45].

The identification of the magnetite ( $\text{Fe}_3\text{O}_4$ ) and maghemite ( $\gamma\text{-Fe}_2\text{O}_3$ ) phases by XRD is quite complex, as both have the same spinel-like cubic crystal structure and therefore exhibit similar diffraction patterns. One way to determine the predominant crystalline phase is to use the peak position corresponding to the crystalline plane (440), with a value of  $62.5^\circ$  for the magnetite phase and  $62.9^\circ$  for maghemite [46]. The samples synthesized here have this peak located at  $62.8^\circ$ , indicating the presence of both phases.

The mean crystallite size ( $D_{DRX}$ ) was calculated from the width at half height of the highest intensity peak (FWHM) from the Scherrer equation (Equation (1)).

$$D_{DRX} = \frac{0.9\lambda}{\beta \cos \theta} \quad (1)$$

where: 0.9 is the proportionality constant for the spherical shape of the particles;  $\lambda$  is the wavelength of radiation  $\text{CuK}\alpha$  ( $1.54056 \text{ \AA}$ );  $\beta$  is the half-height peak width corrected by the standard sample;  $\theta$  is the Bragg diffraction angle of the most intense peak relative to the reflection of the crystalline plane (311).

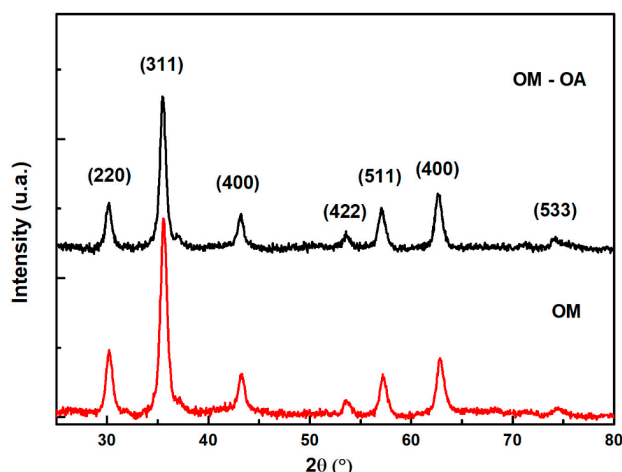


**Figure 1.** X-ray diffractograms of samples of magnetic oxide (OM) and oleic acid functionalized magnetic oxide (OM-OA).

The average crystallite sizes obtained were 10.5 nm (OM) and 12.2 nm (OM-OA), this increase was also observed in other studies [47–49]. These values are important from the point of view of application in intravascular embolization, since the superparamagnetic character is essential for this medical procedure and is characteristic of particles with an average size smaller than the critical size, generally agreed to be less than 20 nm [50].

Figure 2 shows the magnetization curve of OM and OM-OA samples as a function of the applied field at room temperature. The saturation magnetization ( $M_s$ ) of the OM and OM-OA samples were 63.7 and 57.4  $\text{emu}\cdot\text{g}^{-1}$ , respectively. The OM-OA sample shows a lower  $M_s$  value compared to the OM sample, a reduction of approximately 10.4%. This decrease can be explained by the fact that the value of this measurement corresponds to the sum of all magnetic moments present in the sample, in this case, the magnetic material (iron oxides) and the non-magnetic coating material (oleic acid). Thus, this result shows that the non-magnetic coating layer present in the OM-OA sample has a ratio of approximately 10%. In addition, the nanoparticles showed superparamagnetic behavior, since the coercivity and magnetization values of remnant are close to zero [51], corroborating the XRD results. Thus, besides the fact that the  $\text{Fe}_3\text{O}_4$  nanoparticles become hydrophobic, the chemical functionalization of the magnetic oxide surfaces with oleic acid preserved the magnetic properties.

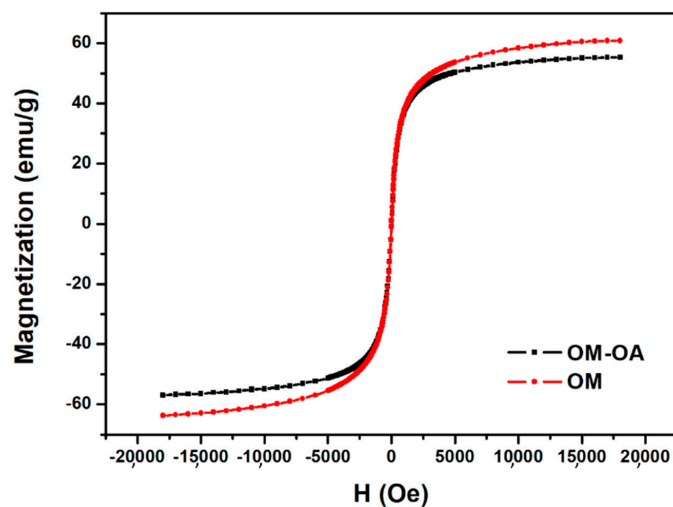


**Figure 2.** Magnetization curves as a function of the magnetic field applied at room temperature of samples OM and OM-OA.

PMMA/OM-OA nanocomposites were obtained by in situ incorporation of OM-OA nanoparticles into poly(methyl methacrylate) matrices by miniemulsion technique. This polymerization process favors the formation of high molar mass lattices, narrow particle size distributions, high colloidal stability and proper encapsulation of inorganic nanoparticles [27]. All miniemulsions were prepared with 15% monomer phase (MMA) and 15% by weight OM-OA relative to monomer content. In addition, 3% by weight hexadecane and 2% initiator (BPO), both relative to monomer mass.

Figure 3 shows the micrographs from TEM measurements and histogram of sample size distribution (A) PMMA and (B) PMMA/PVPi. The particles showed spherical morphology and uniform size, where 326 and 307 particles were analyzed and found average sizes of  $70 \pm 10$  nm and  $85 \pm 9$  nm for PMMA and PMMA/PVPi respectively. Figure 3 clearly shows that a core-structure type structure was properly obtained through seeded emulsion polymerization by using precursor PMMA nanoparticles from miniemulsion polymerization process. According to average particle size, the fraction of PVPi in the outer shell of polymer particles is expected to be in the interval from approximately 14.3 wt.% to 19.0 wt.%, which agrees very well with the theoretical PVPi mass fraction equal to 17.7% for a total consumption of the vinyl pivalate.

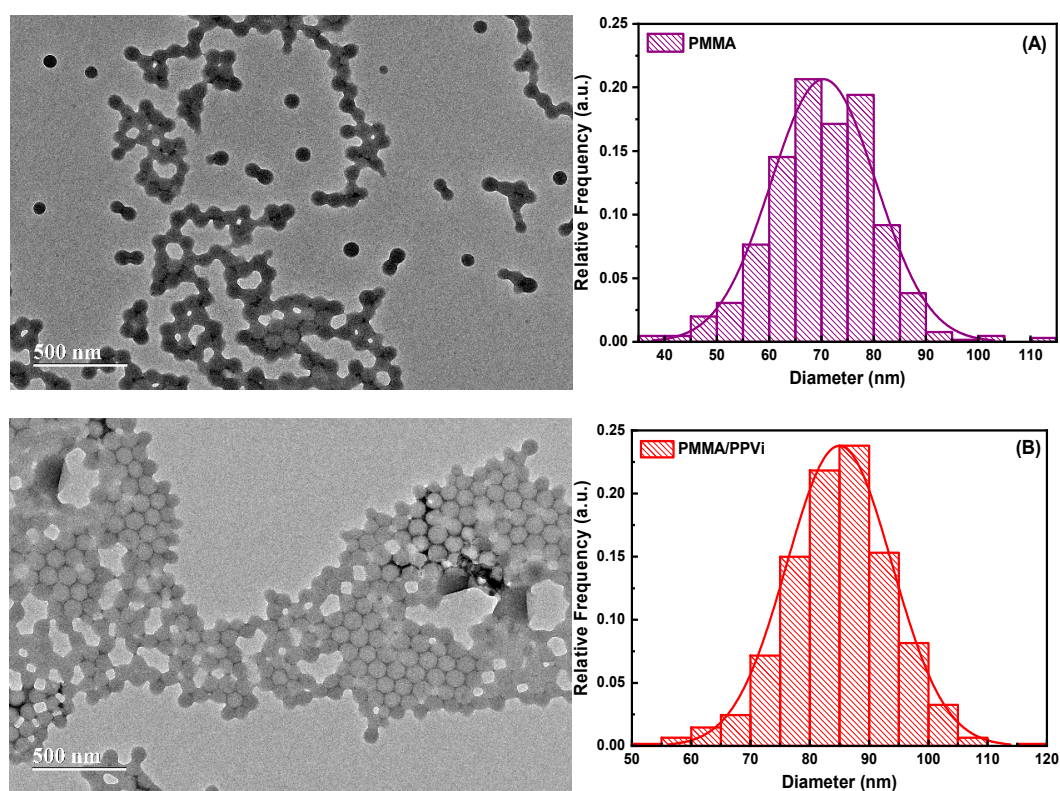


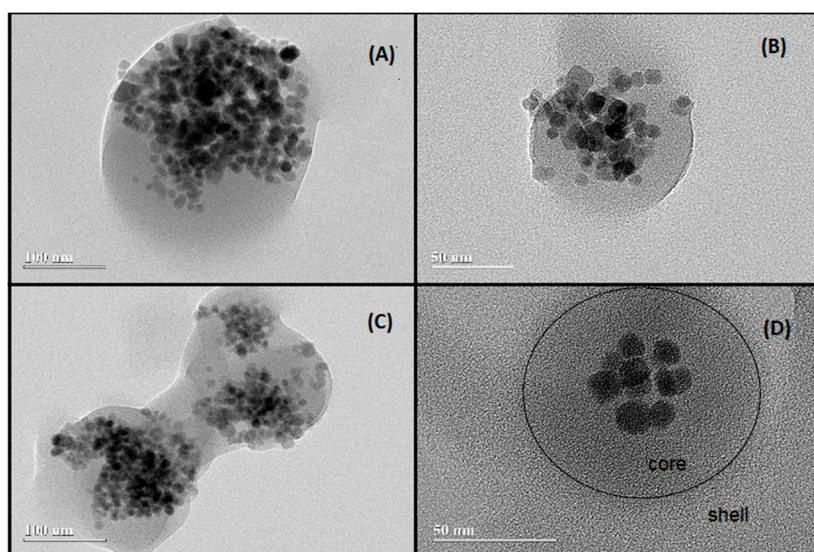
**Figure 3.** Micrographs from TEM measurements and histogram of particle size distribution (A) PMMA homopolymer and (B) PMMA/PVPi core-shell nanoparticles.

In the particular case of magnetic core-shell particles (PMMA/OM-OA and PMMA/OM-OA/PVPi), high conversion was achieved, around 89%, after 2 h of polymerization. Comparatively, using DLS analysis, the polymer particle diameter of the core structure obtained through miniemulsion polymerization remained virtually unchanged, exhibiting 190 nm for monomer droplets ( $D_g$ , with  $PdI = 0.229$ ) and 217 nm polymer particles ( $D_p$ , with  $PdI = 0.254$ ), indicating that the nucleation mechanism preferably occurs within the monomer droplets and that the coalescence and Ostwald ripening effects were minimized during polymerization (N.B.  $PdI$  values around 0.248 indicate that nanoparticles with relatively narrow distribution size are obtained). The average particles size



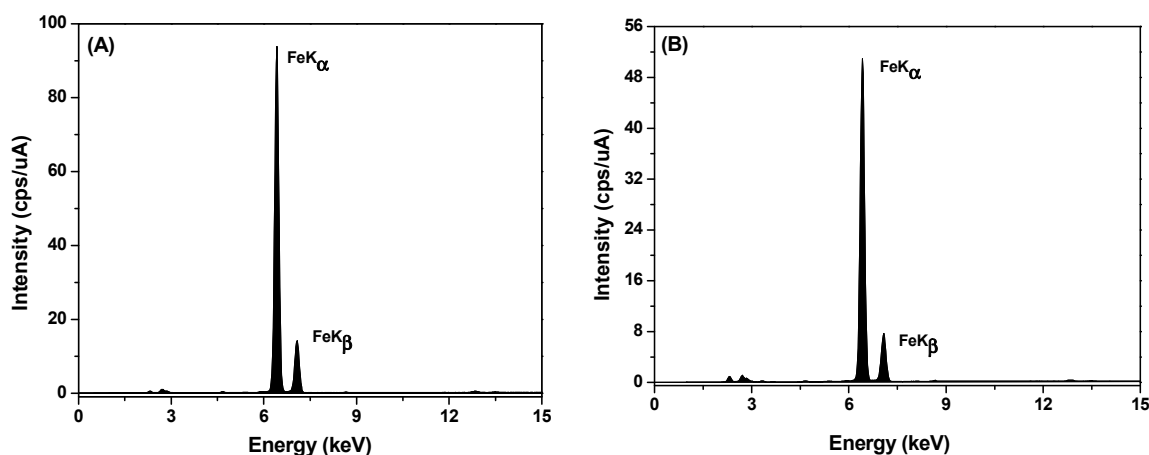
from DLS measurements reveals an increase in the particles diameter as a result of the incorporation of  $\text{Fe}_3\text{O}_4$  magnetic nanoparticles.

Figure 4 shows the TEM of the PMMA/OM-OA and PMMA/OM-OA/PVPi samples, in which it is possible to observe the presence of magnetic nanoparticles uniformly dispersed in spherical polymer nanoparticles, containing an outer layer acquiring a structure of the type core–shell. Figure 4D shows a darker part (core) and a lighter part (shell), showing the formation of a particle with core–shell morphology. Since these are polymers with a close refractive index, the TEM cannot clearly distinguish the shell and core layers. Considering the efficiency of formation of the shell structure and an average number of PMMA/OM-OA equal to  $4.37 \cdot 10^{15}$  particles in the final latex, it is expected to form the final magnetic core–shell particles with an average diameter of approximately 232 nm.



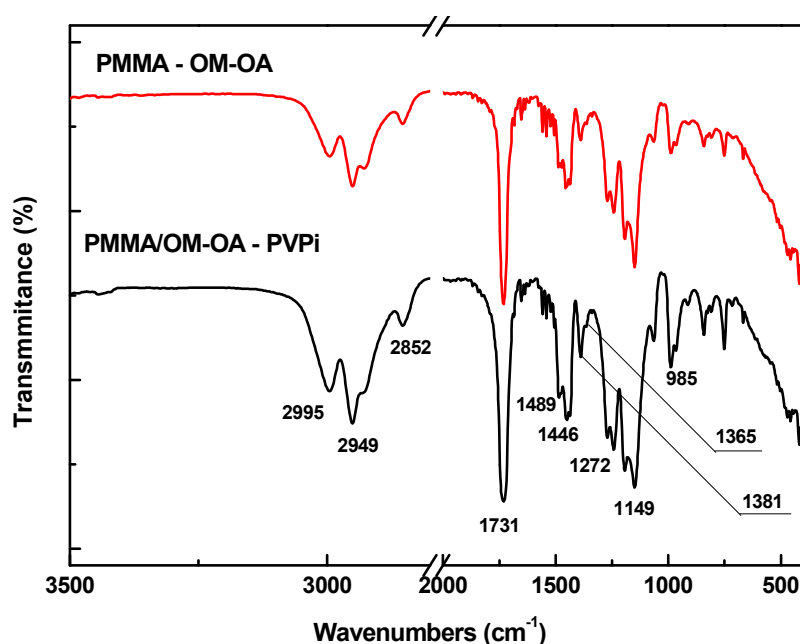
**Figure 4.** (A,B) Micrographs captured by TEM of the PMMA/OM-OA and (C,D) micrographs recorded by TEM of the core–shell poly(methyl methacrylate) nanoparticles (PMMA)/OM-OA/PVPi nanoparticles.

In order to demonstrate that the nanoparticles observed are mainly composed of iron, EDX analysis was performed, being possible to observe the dominant  $\text{K}\alpha$  and  $\text{K}\beta$  peaks related to iron in the interval from 6.40 Kev to 7.06 Kev (Figure 5). The fraction of Fe observed in the samples was approximately 97% along with small amounts of impurities associated with Si, Ca, S, Zn, and Mn from the reagents used in the syntheses. The results observed in Figure 5 are in agreement with the experimental results described elsewhere [17,18].



**Figure 5.** Energy dispersive X-ray spectra of the nanoparticles. (A) PMMA/OM-OA; (B) PMMA/OM-OA/PVPi.

Figure 6 shows the FTIR spectrum of PMMA/OM-OA and PMMA/OM-OA/PVPi samples. The main absorption bands and their respective vibrational assignments are presented in Table 1. The absorption bands between  $2995$  and  $2852$   $\text{cm}^{-1}$  are characteristic of asymmetrical and symmetrical stretching C-H  $\text{sp}^3$ . The peak at  $1731$   $\text{cm}^{-1}$  is attributed to the carbonyl group stretch and the  $1272$  and  $1149$   $\text{cm}^{-1}$  bands to the C-O stretch corresponding to the ester group present in the structure of MMA, VPi, and EGDMA. Absorption at  $1381$  and  $1365$   $\text{cm}^{-1}$  are attributed to the  $-\text{CH}_3$  symmetrical angular deformation of PVi tert-butyl groups [52]. The obtaining of the polymeric material is confirmed by the  $1446$   $\text{cm}^{-1}$  band referring to the angular deformation of the methylene group ( $-\text{CH}_2$ ) of the polymeric chain and the absence of absorption bands between  $3100$  and  $3000$   $\text{cm}^{-1}$  and bands between  $990$  and  $910$   $\text{cm}^{-1}$  attributed, respectively, to the stretching and angular deformation  $\text{CH sp}^2$  of vinyl groups [53]. In the spectra, the presence of magnetic oxides was not confirmed due to the absence of absorption in the  $578$   $\text{cm}^{-1}$  region attributed to Fe-O stretching of tetrahedral sites [54]. Nevertheless, approaching a magnet to the latex shows that the nanoparticles are attracted to the container wall. These results indicate that OM-OA are dispersed in the polymer matrix in a small amount [55].

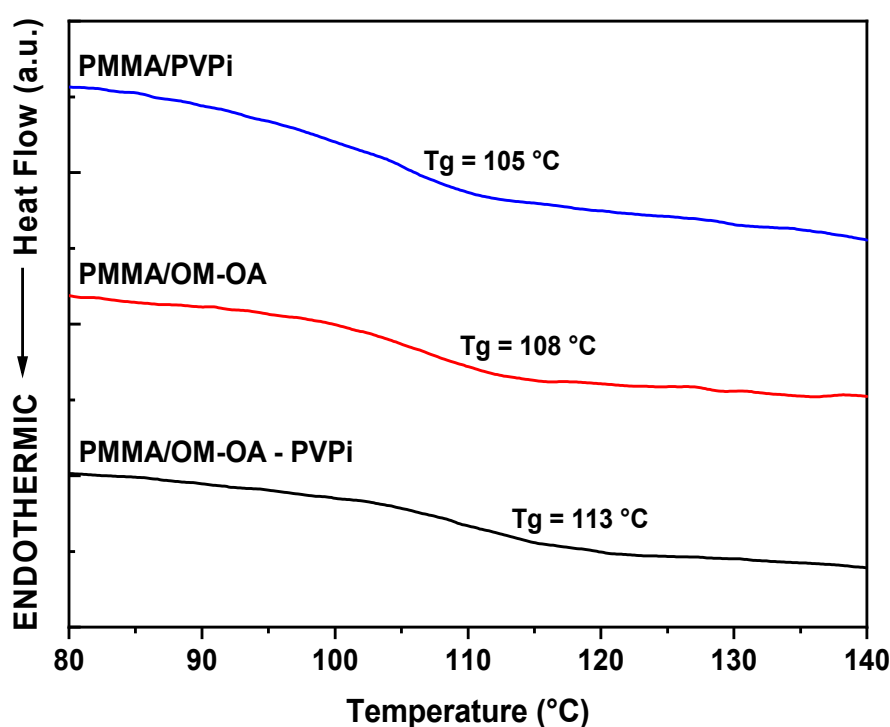


**Figure 6.** FTIR spectra of PMMA/OM-OA and PMMA/OM-OA/PVPi samples obtained from KBr pellets.

**Table 1.** Main absorption bands obtained in FTIR spectra for PMMA/OM-OA and PMMA/OM-OA/PVPi samples and their vibrational assignments.

Wavenumbers (cm <sup>-1</sup> )	Vibrational Assignments
2995–2852	Asymmetrical and symmetrical stretch C-H sp <sup>3</sup>
1731	Stretch C=O of ester
1489 and 1446	Angular deformation of methylene groups (–CH <sub>2</sub> )
1381 and 1365	Symmetrical angular deformation –CH <sub>3</sub> of tert-butyl groups
1272 and 1149	Stretch C-O of ester
985	Out of plane angular deformation C-H

The glass transition temperatures ( $T_g$ ) of PMMA/OM-OA and PMMA/OM-OA/PVPi samples were determined by the DSC curves shown in Figure 7. The  $T_g$  reached values greater than 110 °C, which are higher than those reported in the literature, around 104 °C [56]. This increase is attributed to the presence of OM-OA nanoparticles, restricting the mobility of the polymer chains [57] or due to a change in the tacticity of the PMMA chains [58], with major interactions between polymer chains and, consequently, increasing the  $T_g$  values. The  $T_g$  values of the PMMA/OM-OA nanocomposites were 108 °C, while those of the PMMA/OM-OA/PVPi were 113 °C. It is also worth mentioning that the increase in  $T_g$  observed here for the polymer resulted from seed emulsion process is closely related to the EGDMA used as cross-linking agent.

**Figure 7.** DSC curves of the PMMA/OM-OA and PMMA/OM-OA/poly(vinyl pivalate) (PVPi) samples.

The mass fraction of vinyl pivalate ( $\mathfrak{J}_{VPi}$ ) estimated based on the Fox model (Equation (2)) is equal to 0.16, indicating that vinyl pivalate was successfully incorporated onto the surface of the precursors PMMA particles, which explains the dominant effect of the composition on the  $T_g$  of the copolymers. It is important to emphasize that the DSC measurements corroborate the vinyl pivalate mass fraction estimated from TEM measurements, which was determined to be in the interval from approximately 0.14 to 0.19.

$$\frac{1}{T_{g12}} = \frac{(1 - \mathfrak{J}_{VPi})}{T_{g1}} + \frac{\mathfrak{J}_{VPi}}{T_{g2}} \quad (2)$$

where,  $T_{g1}$ ,  $T_{g2}$  and  $T_{g3}$  are the glass transition temperatures of the PMMA/PVPi, and in the literature of poly(methyl methacrylate) with  $T_g = 110$  °C and poly(vinyl pivalate) with  $T_g = 80$  °C, respectively [59,60].

The magnetic behavior of the PMMA/OM-OA and PMMA/OM-OA/PVPi samples at room temperature is shown in Figure 8. The samples showed saturation magnetization ( $M_s$ ) of  $4.65 \text{ emu} \cdot \text{g}^{-1}$  ( $M_s = 57.4 \text{ emu} \cdot \text{g}^{-1}$  of nanoparticles) and  $1.35 \text{ emu} \cdot \text{g}^{-1}$  ( $56.25 \text{ emu} \cdot \text{g}^{-1}$  of nanoparticles), respectively. The magnetization curves have no hysteresis cycle and are reversible at room temperature, indicating that the superparamagnetic behavior of the nanoparticles was preserved during polymerization and their magnetic properties were successfully incorporated into the nanocomposites.

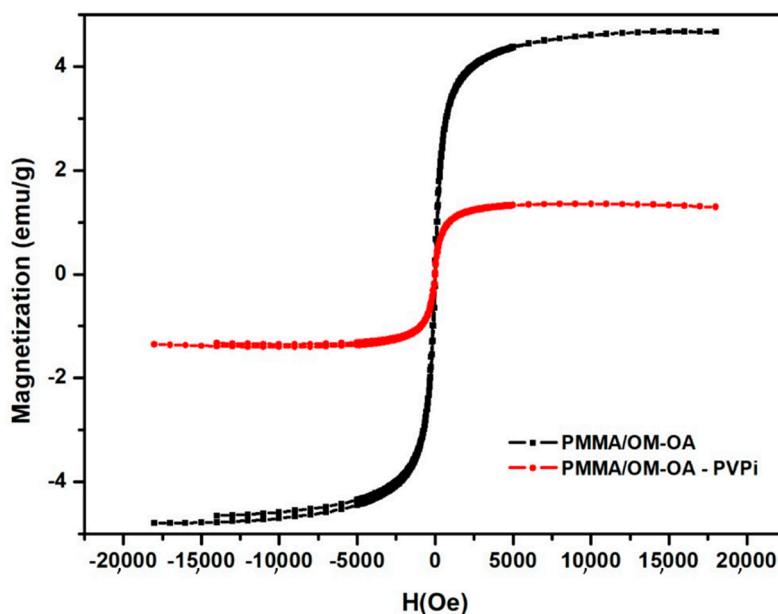


**Figure 8.** Magnetization curves as a function of the magnetic field applied to the ambient temperature of the PMMA/OM-OA and PMMA/OM-OA/PVPi samples.

The  $M_s$  values of the nanocomposites were significantly lower than that of OM-OA ( $M_s = 57.4 \text{ emu} \cdot \text{g}^{-1}$ ), due to the existence of non-magnetic polymeric material present in the samples. Considering these  $M_s$  values, it is possible to have an estimate of the OM and OM-OA content incorporated in each nanocomposite, being, respectively, 7.3% and 8.1% for PMMA/OM-OA and 2.1% and 2.4% for PMMA/OM-OA/PVPi. In fact, these values are slightly higher, since during polymerization part of the magnetic oxides, such as  $\text{Fe}_3\text{O}_4$ , are converted into other iron oxides that have less magnetization, such as  $\gamma\text{-Fe}_2\text{O}_3$ , due to the presence of strong oxidants, such as BPO [17,47]. These  $M_s$  values corroborate the results of FTIR and DSC in which they show the presence of the poly(vinyl pivalate) matrix present in the nanocomposites obtained by seeded emulsion.

Figures 9 and 10 depict cytotoxicity results of in vitro tests performed with polymeric particles. This kind of biological test is of fundamental importance, as it is closely related to product viability, according to its level of toxicity. Considering that both human and animal cells were used, and knowing that lower percentage of cell viability, the greater its cytotoxic potential, it is necessary to evaluate influence of material concentration on cell viability in order to determine its borderline concentration.

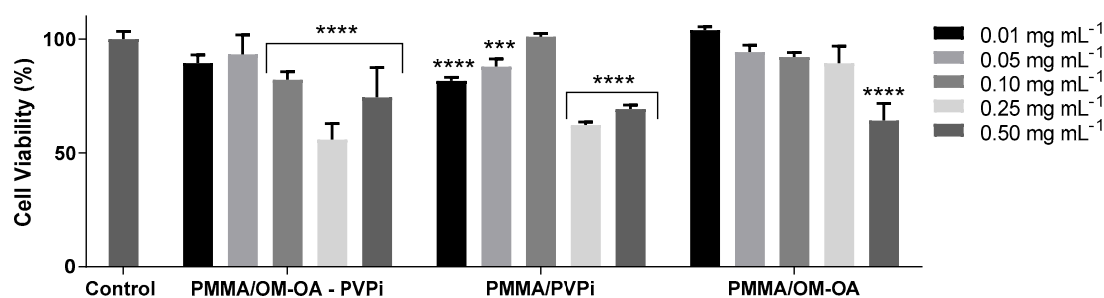


**Figure 9.** Evaluation of cytotoxic activity of poly(methyl methacrylate)/magnetic oxide coated with oleic acid/poly(vinyl pivalate)—(PMMA/OM-OA/PVPI), poly(methyl methacrylate)/poly(vinyl pivalate)—(PMMA/PVPI) and poly(methyl methacrylate)/magnetic oxide coated with oleic acid—(PMMA/OM-OA) in murine melanoma tumor cell lines, B16F10, after 24h exposure in the concentrations of 0.01 mg·mL<sup>-1</sup>, 0.05 mg·mL<sup>-1</sup>, 0.10 mg·mL<sup>-1</sup>, 0.25 mg·mL<sup>-1</sup>, and 0.50 mg·mL<sup>-1</sup>. The asterisks are related to the statistical significance associated with different confidence levels: \* for 95% with  $p \leq 0.05$ , \*\* 99% with  $p \leq 0.01$ , \*\*\* 99.9% with  $p \leq 0.001$  and \*\*\*\* 99.99% with  $p \leq 0.0001$ .

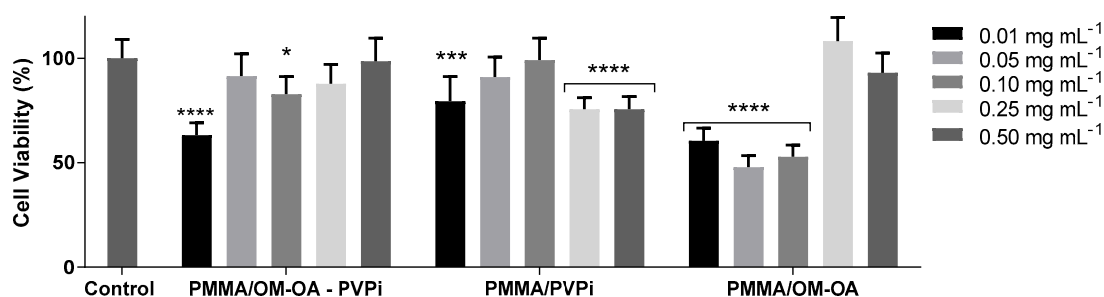


**Figure 10.** Evaluation of cytotoxic activity of poly(methyl methacrylate)/magnetic oxide coated with oleic acid/poly (vinyl pivalate)—(PMMA/OM-OA/PVPI), poly(methyl methacrylate)/poly (vinyl pivalate)—(PMMA/PVPI) and poly(methyl methacrylate)/magnetic oxide coated with oleic acid—(PMMA/OM-OA) in human keratinocyte cells, HaCaT, after 24 h in the concentrations of 0.01 mg·mL<sup>-1</sup>, 0.05 mg·mL<sup>-1</sup>, 0.10 mg·mL<sup>-1</sup>, 0.25 mg·mL<sup>-1</sup>, and 0.50 mg·mL<sup>-1</sup>. The asterisks are related to the statistical significance associated with different confidence levels: \* for 95% with  $p \leq 0.05$ , \*\* 99% with  $p \leq 0.01$ , \*\*\* 99.9% with  $p \leq 0.001$  and \*\*\*\* 99.99% with  $p \leq 0.0001$ .

Figure 9 illustrates performance of tested polymeric materials against murine melanoma tumor line (B16F10) in cell viability at an exposure of 24 h when compared to the control ( $p < 0.05$ ). For each polymeric material, assays were carried out with polymer concentrations lying in interval from 0.01 mg·mL<sup>-1</sup> to 0.50 mg·mL<sup>-1</sup>. According to Figure 9, concentration of polymer samples plays an important effect on cell viability. It is observed that cell viability is slightly affected when low polymer concentrations are employed (i.e., from 0.01 mg·mL<sup>-1</sup> to 0.10 mg·mL<sup>-1</sup>), leading to a decrease in average cell viability of at most 18%. In general for other polymer materials, it seems reasonable to assume that borderline concentration corresponds to concentration of 0.25 mg·mL<sup>-1</sup>, which leads to a decrease in cell viability of approximately 45%. It is also important to bear in mind that best results were observed for core-shell magnetic polymer materials (PMMA/OM-OA and PMMA/OM-OA/PVPI), presenting a cell viability comparable to control, at concentrations of 0.01 to 0.25 mg·mL<sup>-1</sup> and from 0.01 and 0.05 mg·mL<sup>-1</sup>, respectively. This result is very promising, considering that as an embolic agent this versatile material present a twofold action, as they can be used to both obstruct blood vessels interrupting supply of oxygen and nutrients to tumor region and hyperthermia treatment of injured area.

A similar study has been carried out for HaCaT lineage in order to evaluate the polymer materials toxicity to non-pathological cells. According to Figure 10, target magnetic polymer with core-shell structure (PMMA/OM-OA/PVPI) exhibits highest cell viability in comparison to the other

tested polymer materials, and whose values of cell viability can be considered comparable and very close to control, except for concentration of  $0.01 \text{ mg}\cdot\text{mL}^{-1}$ . It is also interesting to notice that PMMA/OM-OA/PVPi performance seems not to be dependent on concentration in experimental range evaluated here. In particular case of poly(methyl methacrylate) magnetic particles (PMMA/OM-OA), high cell viability were observed for concentration of  $0.25 \text{ mg}\cdot\text{mL}^{-1}$  and  $0.50 \text{ mg}\cdot\text{mL}^{-1}$  equivalent to 108% and 93%, respectively.

Non-magnetic core-shell nanoparticles (PMMA/PVPi) presented an average cell viability of 84%; however, the highest cell viability very close control was approximately 99% observed for concentration of  $0.10 \text{ mg}\cdot\text{mL}^{-1}$ .

Feuser et al. [61] evaluated in vitro cytotoxicity in murine fibroblast (L929) and normal human fibroblast (NIH-3T3) by MTT assay for 24 h of PMMA nanoparticles and nanocapsules obtained by miniemulsion polymerization. Both cells presented high cell viability, between 81 to 84% even at highest tested concentration of  $750 \mu\text{g}\cdot\text{mL}^{-1}$ . Guindani et al. [62] also investigated in vitro cytotoxicity in mouse embryonic fibroblasts (NIH3T3) breast cancer (MDAMB231) and human cervical cancer (HeLa) by MTT assay for 24 h of PMMA nanoparticles and nanocapsules of PMMA conjugated with bovine serum albumin (BSA) obtained by miniemulsion polymerization at four concentrations: 100, 200, 300, and  $400 \mu\text{g}\cdot\text{mL}^{-1}$ . According to authors, polymeric materials can be considered biocompatible in all concentrations tested. Mendes et al. [63] evaluated cytotoxic activity of PMMA nanoparticles obtained by miniemulsion polymerization in human leukemic cell line K562 by MTT assay for 24 h. Cytotoxic activity of polymeric nanoparticles did not induce cell death even at highest tested concentration of  $1500 \mu\text{g}\cdot\text{mL}^{-1}$ .

According the Chinese standard (GB/T 16886.5-2003) materials with cell viability greater than 75% represent no cytotoxicity [64,65]. Therefore, based on the results obtained in this study, it is possible to consider that nanoparticles achieved high cell viability for both murine melanoma tumor cell lines, B16F10, and human keratinocyte cells, HaCaT., and can be considered promising for other biological studies such as in vivo tests.

#### 4. Conclusions

The results showed that functionalized magnetic nanoparticles presented good dispersibility with a uniform average size of 10.5 nm, saturation magnetization of  $57.4 \text{ emu}\cdot\text{g}^{-1}$  and superparamagnetic behavior. Miniemulsion polymerization process ensured that magnetic nanoparticles were encapsulated in polymer matrix uniformly, maintaining their superparamagnetic properties with  $56.25 \text{ emu}\cdot\text{g}^{-1}$  of  $\text{Fe}_3\text{O}_4$  nanoparticles. Results obtained are promising, since from point of view of medical application of intravascular embolization. Superparamagnetic character, essential for this medical procedure, remains present in nanocomposite and in result of seeded emulsion, in addition to presence of core-shell morphology. This new polymeric material designed to contain, as a core-shell structure, poly(methyl methacrylate)/magnetic  $\text{Fe}_3\text{O}_4$ /poly(vinyl pivalate), exhibited high colloidal stability, which can be linked to the desired properties of methyl methacrylate/vinyl pivalate-based polymers such as good chemical, mechanical and thermal stability.

Based on cell viability assays, the core-shell magnetic polymeric materials [a core, consisting of poly(methyl methacrylate)/ $\text{Fe}_3\text{O}_4$  and a shell, formed by poly(vinyl pivalate)] can be regarded as a very promising material, as they achieved high cell viabilities for both murine melanoma tumor cell lines, B16F10, and human keratinocyte cells, HaCaT.

**Author Contributions:** F.M. and S.B.C. conceived and designed the experiments; G.R., G.V.S.D., and M.S.B.N. performed the experiments; G.R., G.V.S.D, M.S.B.N., O.A.A., S.B.C., and F.M. analyzed the data and wrote the paper. All authors have read and agreed to the published version of the manuscript.

**Funding:** This research received no external funding.

**Acknowledgments:** This work has been supported by Fundação de Apoio à Pesquisa do Distrito Federal (FAPDF), Conselho Nacional de Desenvolvimento Científico e Tecnológico (CNPq) and Coordenação de Aperfeiçoamento

de Pessoal de Nível Superior (CAPES)—Finance Code 001. The authors thank the Laboratório Multiusuário de Microscopia de Alta Resolução (LabMic) for the TEM micrographs.

**Conflicts of Interest:** The authors declare no conflict of interest.

## References

1. Dutra, G.V.S.; Neto, W.S.; Dutra, J.P.S.; Machado, F. Implantable medical devices and tissue engineering: An overview of manufacturing processes and the use of polymeric matrices for manufacturing and coating their surfaces. *Curr. Med. Chem.* **2020**, *27*, 1580–1599. [[CrossRef](#)] [[PubMed](#)]
2. Teo, A.J.T.; Mishra, A.; Park, I.; Kim, Y.-J.; Park, W.-T.; Yoon, Y.-J. Polymeric Biomaterials for Medical Implants and Devices. *ACS Biomater. Sci. Eng.* **2016**, *2*, 454–472. [[CrossRef](#)]
3. Chen, X.; Lv, H.; Ye, M.; Wang, S.; Ni, E.; Zeng, F.; Cao, C.; Luo, F.; Yan, J. Novel superparamagnetic iron oxide nanoparticles for tumor embolization application: Preparation, characterization and double targeting. *Int. J. Pharm.* **2012**, *426*, 248–255. [[CrossRef](#)] [[PubMed](#)]
4. Rittikulsittichai, S.; Singhana, B.; Bryan, W.W.; Sarangi, S.; Jamison, A.C.; Brazdeikis, A.; Lee, T.R. Preparation, characterization, and utilization of multi-functional magnetic-fluorescent composites for bio-imaging and magnetic hyperthermia therapy. *RSC Adv.* **2013**, *3*, 7838–7849. [[CrossRef](#)]
5. Liu, Z.; Liu, Y.; Shen, S.; Wu, D. Progress of recyclable magnetic particles for biomedical applications. *J. Mater. Chem. B* **2018**, *6*, 366–380. [[CrossRef](#)]
6. Chatterjee, K.; Sarkar, S.; Jagajjanani Rao, K.; Paria, S. Core/shell nanoparticles in biomedical applications. *Adv. Colloid Interface Sci.* **2014**, *209*, 8–39. [[CrossRef](#)]
7. Jiang, Q.L.; Zheng, S.W.; Hong, R.Y.; Deng, S.M.; Guo, L.; Hu, R.L.; Gao, B.; Huang, M.; Cheng, L.F.; Liu, G.H.; et al. Folic acid-conjugated Fe<sub>3</sub>O<sub>4</sub> magnetic nanoparticles for hyperthermia and MRI in vitro and in vivo. *Appl. Surf. Sci.* **2014**, *307*, 224–233. [[CrossRef](#)]
8. Bakhtiyari, Z.; Saei, A.A.; Hajipour, M.J.; Raoufi, M.; Vermesh, O.; Mahmoudi, M. Targeted superparamagnetic iron oxide nanoparticles for early detection of cancer: Possibilities and challenges. *Nanomedicine* **2016**, *12*, 287–307. [[CrossRef](#)]
9. Khan, I.; Saeed, K.; Khan, I. Nanoparticles: Properties, applications and toxicities. *Arab. J. Chem.* **2019**, *12*, 908–931. [[CrossRef](#)]
10. Jun, Y.-W.; Huh, Y.-M.; Choi, J.-S.; Lee, J.-H.; Song, H.-T.; Kim, S.; Yoon, S.; Kim, K.-S.; Shin, J.-S.; Suh, J.-S.; et al. Nanoscale Size Effect of Magnetic Nanocrystals and Their Utilization for Cancer Diagnosis via Magnetic Resonance Imaging. *J. Am. Chem. Soc.* **2005**, *127*, 5732–5733. [[CrossRef](#)]
11. Singh, A.P.; Biswas, A.; Shukla, A.; Maiti, P. Targeted therapy in chronic diseases using nanomaterial-based drug delivery vehicles. *Signal Transduc. Target. Ther.* **2019**, *4*, 33. [[CrossRef](#)] [[PubMed](#)]
12. Zhao, H.; Lin, Z.Y.; Yildirimer, L.; Dhinakar, A.; Zhao, X.; Wu, J. Polymer-based nanoparticles for protein delivery: Design, strategies and applications. *J. Mater. Chem. B* **2016**, *4*, 4060–4071. [[CrossRef](#)] [[PubMed](#)]
13. Li, P.; Zhu, A.M.; Liu, Q.L.; Zhang, Q.G. Fe<sub>3</sub>O<sub>4</sub>/poly(N-Isopropylacrylamide)/Chitosan Composite Microspheres with Multiresponsive Properties. *Ind. Eng. Chem. Res.* **2008**, *47*, 7700–7706. [[CrossRef](#)]
14. Koo, H.Y.; Chang, S.T.; Choi, W.S.; Park, J.-H.; Kim, D.-Y.; Velev, O.D. Emulsion-Based Synthesis of Reversibly Swellable, Magnetic Nanoparticle-Embedded Polymer Microcapsules. *Chem. Mater.* **2006**, *18*, 3308–3313. [[CrossRef](#)]
15. Rouhi, M.; Mansour Lakouraj, M.; Baghayeri, M.; Hasantabar, V. Novel conductive magnetic nanocomposite based on poly(indole-co-thiophene) as a hemoglobin diagnostic biosensor: Synthesis, characterization and physical properties. *Int. J. Polymer. Mater.* **2017**, *66*, 12–19. [[CrossRef](#)]
16. Neves, J.S.; Souza Júnior, F.G.; Suarez, P.A.Z.; Umpierre, A.P.; Machado, F. In situ Production of Polystyrene Magnetic Nanocomposites through a Batch Suspension Polymerization Process. *Macromol. Mater. Eng.* **2011**, *296*, 1107–1118. [[CrossRef](#)]
17. Araujo, R.T.; Ferreira, G.R.; Segura, T.; Souza, F.G.; Machado, F. An experimental study on the synthesis of poly(vinyl pivalate)-based magnetic nanocomposites through suspension polymerization process. *Eur. Polym. J.* **2015**, *68*, 441–459. [[CrossRef](#)]
18. Ferreira, G.R.; Segura, T.; Souza, F.G.; Umpierre, A.P.; Machado, F. Synthesis of poly(vinyl acetate)-based magnetic polymer microparticles. *Eur. Polym. J.* **2012**, *48*, 2050–2069. [[CrossRef](#)]

19. Piazza, R.D.; Nunes, E.S.; Viali, W.R.; Silva, S.W.; Aragón, F.H.; Coaquira, J.A.H.; Morais, P.C.; Marques, R.F.C.; Jafelicci, M. Magnetic nanohydrogel obtained by miniemulsion polymerization of poly(acrylic acid) grafted onto derivatized dextran. *Carbohydr. Polym.* **2017**, *178*, 378–385. [[CrossRef](#)]
20. Gao, F.; Wu, X.; Wu, D.; Yu, J.; Yao, J.; Qi, Q.; Cao, Z.; Cui, Q.; Mi, Y. Preparation of degradable magnetic temperature- and redox-responsive polymeric/Fe<sub>3</sub>O<sub>4</sub> nanocomposite nanogels in inverse miniemulsions for loading and release of 5-fluorouracil. *Colloids Surf. A Physicochem. Eng. Asp.* **2020**, *587*, 124363. [[CrossRef](#)]
21. Chiaradia, V.; Valério, A.; Feuser, P.E.; Oliveira, D.; Araújo, P.H.H.; Sayer, C. Incorporation of superparamagnetic nanoparticles into poly(urea-urethane) nanoparticles by step growth interfacial polymerization in miniemulsion. *Colloids Surf. A Physicochem. Eng. Asp.* **2015**, *482*, 596–603. [[CrossRef](#)]
22. Goode, J.A.; Matson, M.B. Embolisation of cancer: What is the evidence? *Cancer Imaging* **2004**, *4*, 133–141. [[CrossRef](#)] [[PubMed](#)]
23. Coldwell, D.M.; Stokes, K.R.; Yakes, W.F. Embolotherapy: Agents, clinical applications, and techniques. *Radiographics* **1994**, *14*, 623–643. [[CrossRef](#)] [[PubMed](#)]
24. Schwaner, S.L.; Haug, S.B.; Matsumoto, A.H. Overview of embolotherapy: Agents, indications, applications, and nursing management. *Periop. Nurs. Clin.* **2010**, *5*, 137–176. [[CrossRef](#)]
25. Asua, J.M. Challenges for industrialization of miniemulsion polymerization. *Progr. Polym. Sci.* **2014**, *39*, 1797–1826. [[CrossRef](#)]
26. Asua, J.M. Miniemulsion polymerization. *Progr. Polym. Sci.* **2002**, *27*, 1283–1346. [[CrossRef](#)]
27. Crespy, D.; Landfester, K. Miniemulsion polymerization as a versatile tool for the synthesis of functionalized polymers. *Beilstein J. Org. Chem.* **2010**, *6*, 1132–1148. [[CrossRef](#)]
28. Gharieh, A.; Khoei, S.; Mahdavian, A.R. Emulsion and miniemulsion techniques in preparation of polymer nanoparticles with versatile characteristics. *Adv. Colloid Interface Sci.* **2019**, *269*, 152–186. [[CrossRef](#)]
29. Ramli, R.A.; Laftah, W.A.; Hashim, S. Core-shell polymers: A review. *RSC Adv.* **2013**, *3*, 15543–15565. [[CrossRef](#)]
30. Stubbs, J.; Tsavalas, J.; Carrier, R.; Sundberg, D. The Structural Evolution of Composite Latex Particles During Starve-Fed Emulsion Polymerization: Modeling and Experiments for Kinetically Frozen Morphologies. *Macromol. React. Eng.* **2010**, *4*, 424–431. [[CrossRef](#)]
31. Pei, X.; Zhai, K.; Tan, Y.; Xu, K.; Lu, C.; Wang, P.; Wang, T.; Chen, C.; Tao, Y.; Dai, L.; et al. Synthesis of monodisperse starch-polystyrene core-shell nanoparticles via seeded emulsion polymerization without stabilizer. *Polymer* **2017**, *108*, 78–86. [[CrossRef](#)]
32. Law, W.-C.; Yong, K.-T.; Roy, I.; Xu, G.; Ding, H.; Bergey, E.J.; Zeng, H.; Prasad, P.N. Optically and magnetically doped organically modified silica nanoparticles as efficient magnetically guided biomarkers for two-photon imaging of live cancer cells. *J. Phys. Chem. C* **2008**, *112*, 7972–7977. [[CrossRef](#)]
33. Nagarajan, S.; Yong, Z. Use of core/shell structured nanoparticles for biomedical applications. *Recent Pat. Biomed. Eng.* **2008**, *1*, 34–42.
34. Rahman, M.M.; Chehimi, M.M.; Fessi, H.; Elaissari, A. Highly temperature responsive core-shell magnetic particles: Synthesis, characterization and colloidal properties. *J. Colloid Interface Sci.* **2011**, *360*, 556–564. [[CrossRef](#)]
35. Chen, L.; Hong, L.; Lin, J.-C.; Meyers, G.; Harris, J.; Radler, M. Epoxy-acrylic core-shell particles by seeded emulsion polymerization. *J. Colloid Interface Sci.* **2016**, *473*, 182–189. [[CrossRef](#)]
36. Li, Y.; Chen, S.; Demirci, S.; Qin, S.; Xu, Z.; Olson, E.; Liu, F.; Palm, D.; Yong, X.; Jiang, S. Morphology evolution of Janus dumbbell nanoparticles in seeded emulsion polymerization. *J. Colloid Interface Sci.* **2019**, *543*, 34–42. [[CrossRef](#)]
37. Li, W.S.J.; Ladmiral, V.; Takeshima, H.; Satoh, K.; Kamigaito, M.; Semsarilar, M.; Negrell, C.; Lacroix-Desmazes, P.; Caillol, S. Ferulic acid-based reactive core-shell latex by seeded emulsion polymerization. *Polym. Chem.* **2019**, *10*, 3116–3126. [[CrossRef](#)]
38. Mock, E.B.; De Bruyn, H.; Hawkett, B.S.; Gilbert, R.G.; Zukoski, C.F. Synthesis of anisotropic nanoparticles by seeded emulsion polymerization. *Langmuir* **2006**, *22*, 4037–4043. [[CrossRef](#)]
39. Wichaita, W.; Polpanich, D.; Suteewong, T.; Tangboriboonrat, P. Hollow core-shell particles via NR latex seeded emulsion polymerization. *Polymer* **2016**, *99*, 324–331. [[CrossRef](#)]
40. Lyu, S.; Untereker, D. Degradability of polymers for implantable biomedical devices. *Int. J. Mol. Sci.* **2009**, *10*, 4033–4065. [[CrossRef](#)]
41. Hsu, S.L. Poly(methyl methacrylate). In *Polymer Data Handbook*; Mark, J.E., Ed.; Oxford University Press, Inc.: Oxford, UK, 1999; pp. 655–657.



42. Neto, W.S.; Dutra, G.V.S.; Jensen, A.T.; Araújo, O.A.; Garg, V.; Oliveira, A.C.; Valadares, L.F.; Souza, F.G.; Machado, F. Superparamagnetic nanoparticles stabilized with free-radical polymerizable oleic acid-based coating. *J. Alloys Compd.* **2018**, *739*, 1025–1036. [[CrossRef](#)]
43. Jensen, A.T.; Sayer, C.; Araújo, P.H.H.; Machado, F. Emulsion copolymerization of styrene and acrylated methyl oleate. *Eur. J. Lipid Sci. Technol.* **2014**, *116*, 37–43. [[CrossRef](#)]
44. Tang, P.L.; Sudol, E.D.; Adams, M.; El-Aasser, M.S.; Asua, J.M. Seeded emulsion polymerization of *n*-butyl acrylate utilizing miniemulsions. *J. Appl. Polym. Sci.* **1991**, *42*, 2019–2028. [[CrossRef](#)]
45. Lobato, N.C.C.; Mansur, M.B.; Ferreira, A.M. Characterization and Chemical Stability of Hydrophilic and Hydrophobic Magnetic Nanoparticles. *Mater. Res.* **2017**, *20*, 736–746. [[CrossRef](#)]
46. Araújo-Neto, R.P.; Silva-Freitas, E.L.; Carvalho, J.F.; Pontes, T.R.F.; Silva, K.L.; Damasceno, I.H.M.; Egito, E.S.T.; Dantas, A.L.; Morales, M.A.; Carriço, A.S. Monodisperse sodium oleate coated magnetite high susceptibility nanoparticles for hyperthermia applications. *J. Magn. Magn. Mater.* **2014**, *364*, 72–79. [[CrossRef](#)]
47. Feuser, P.E.; Bubniak, L.d.S.; Silva, M.C.d.S.; Viegas, A.d.C.; Castilho Fernandes, A.; Ricci-Junior, E.; Nele, M.; Tedesco, A.C.; Sayer, C.; de Araújo, P.H.H. Encapsulation of magnetic nanoparticles in poly(methyl methacrylate) by miniemulsion and evaluation of hyperthermia in U87MG cells. *Eur. Polym. J.* **2015**, *68*, 355–365. [[CrossRef](#)]
48. Klencsár, Z.; Ábrahám, A.; Szabó, L.; Szabó, E.G.; Stichleutner, S.; Kuzmann, E.; Homonnay, Z.; Tolnai, G. The effect of preparation conditions on magnetite nanoparticles obtained via chemical co-precipitation. *Mater. Chem. Phys.* **2019**, *223*, 122–132. [[CrossRef](#)]
49. Dutra, G.V.S.; Araújo, O.A.; Neto, W.S.; Garg, V.K.; Oliveira, A.C.; Júnior, A.F. Obtaining superhydrophobic magnetic nanoparticles applicable in the removal of oils on aqueous surface. *Mater. Chem. Phys.* **2017**, *200*, 204–216. [[CrossRef](#)]
50. Li, Q.; Kartikowati, C.W.; Horie, S.; Ogi, T.; Iwaki, T.; Okuyama, K. Correlation between particle size/domain structure and magnetic properties of highly crystalline Fe<sub>3</sub>O<sub>4</sub> nanoparticles. *Sci. Rep.* **2017**, *7*, 9894–9900. [[CrossRef](#)]
51. Wahajuddin; Arora, S. Superparamagnetic iron oxide nanoparticles: Magnetic nanoplatforms as drug carriers. *Int. J. Nanomed.* **2012**, *7*, 3445–3471. [[CrossRef](#)]
52. Islam, N.; Haldorai, Y.; Nguyen, V.H.; Shim, J.-J. Synthesis of poly(vinyl pivalate) by atom transfer radical polymerization in supercritical carbon dioxide. *Eur. Polym. J.* **2014**, *61*, 93–104. [[CrossRef](#)]
53. Pavia, D.L.; Lampman, G.M.; Kriz, G.S.; Vyvyan, J.A. *Introduction to Spectroscopy*; Cengage Learning: Boston, MA, USA, 2008.
54. Lei, W.; Liu, Y.; Si, X.; Xu, J.; Du, W.; Yang, J.; Zhou, T.; Lin, J. Synthesis and magnetic properties of octahedral Fe<sub>3</sub>O<sub>4</sub> via a one-pot hydrothermal route. *Phys. Lett. A* **2017**, *381*, 314–318. [[CrossRef](#)]
55. Qiu, G.; Wang, Q.; Wang, C.; Lau, W.; Guo, Y. Polystyrene/Fe<sub>3</sub>O<sub>4</sub> magnetic emulsion and nanocomposite prepared by ultrasonically initiated miniemulsion polymerization. *Ultrasound. Sonochem.* **2007**, *14*, 55–61. [[CrossRef](#)] [[PubMed](#)]
56. Brandrup, J.; Immergut, E.H.; Grulke, E.A. *Polymer Handbook*, 4th ed.; Wiley-Blackwell: New York, NY, USA, 1999.
57. Barandiaran, I.; Kortaberria, G. Magnetic nanocomposites based on poly(styrene-*b*-butadiene-*b*-methyl methacrylate) and modified Fe<sub>2</sub>O<sub>3</sub> nanoparticles. *Eur. Polym. J.* **2016**, *78*, 340–351. [[CrossRef](#)]
58. Norakankorn, C.; Pan, Q.; Rempel, G.L.; Kiatkamjornwong, S. Synthesis of poly(methyl methacrylate) nanoparticles initiated by azobisisobutyronitrile using a differential microemulsion polymerization technique. *J. Appl. Polym. Sci.* **2009**, *113*, 375–382. [[CrossRef](#)]
59. Billmeyer, F.W. *Textbook of Polymer Science*; Wiley-Interscience: New York, NY, USA, 1984.
60. Jensen, A.T.; Oliveira, A.C.C.; Gonçalves, S.B.; Gambetta, R.; Machado, F. Evaluation of the emulsion copolymerization of vinyl pivalate and methacrylated methyl oleate. *J. Appl. Polym. Sci.* **2016**, *133*, 44129–44139. [[CrossRef](#)]
61. Feuser, P.E.; Bubniak, L.S.; Bodack, C.N.; Valério, A.; Santos-Silva, M.C.; Ricci-Junior, E.; Sayer, C.; Araújo, P.H.H. In vitro cytotoxicity of poly(methyl methacrylate) nanoparticles and nanocapsules obtained by miniemulsion polymerization for drug delivery application. *J. Nanosci. Nanotechnol.* **2016**, *16*, 7669–7676. [[CrossRef](#)]

62. Guindani, C.; Feuser, P.E.; Cordeiro, A.P.; de Meneses, A.C.; Possato, J.C.; da Silva Abel, J.; Machado-de-Ávila, R.A.; Sayer, C.; de Araújo, P.H.H. Bovine serum albumin conjugation on poly(methyl methacrylate) nanoparticles for targeted drug delivery applications. *J. Drug Deliv. Sci. Technol.* **2020**, *56*, 101490. [[CrossRef](#)]
63. Mendes, A.N.; Filgueiras, L.A.; Siqueira, M.R.P.; Barbosa, G.M.; Holandino, C.; de Lima Moreira, D.; Pinto, J.C.; Nele, M. Encapsulation of Piper cabralanum (Piperaceae) nonpolar extract in poly(methyl methacrylate) by miniemulsion and evaluation of increase in the effectiveness of antileukemic activity in K562 cells. *Int. J. Nanomed.* **2017**, *12*, 8363–8373. [[CrossRef](#)]
64. Shanmugam, S.; Gopal, B. Antimicrobial and cytotoxicity evaluation of aliovalent substituted hydroxyapatite. *Appl. Surf. Sci.* **2014**, *303*, 277–281. [[CrossRef](#)]
65. Morozov, A.G.; Razborov, D.A.; Egiazaryan, T.A.; Baten'kin, M.A.; Aleynik, D.Y.; Egorikhina, M.N.; Rubtsova, Y.P.; Charikova, I.N.; Chesnokov, S.A.; Fedushkin, I.L. In Vitro Study of Degradation Behavior, Cytotoxicity, and Cell Adhesion of the Atactic Polylactic Acid for Biomedical Purposes. *J. Polym. Environ.* **2020**, *28*, 2652–2660. [[CrossRef](#)]

**Publisher's Note:** MDPI stays neutral with regard to jurisdictional claims in published maps and institutional affiliations.



© 2020 by the authors. Licensee MDPI, Basel, Switzerland. This article is an open access article distributed under the terms and conditions of the Creative Commons Attribution (CC BY) license (<http://creativecommons.org/licenses/by/4.0/>).